Research article

Cardiac toxicity of *Triptergium wilfordii* Hook F. may correlate with its inhibition to hERG channel

Wei Zhao [a,b,1], Liping Xiao [a,b,1], Lanying Pan [a,b], Xianfu Ke [c], Yanting Zhang [a,b], Dian Zhong [a,b], Jianwei Xu [a,b], Fumin Cao [a,b], Liren Wu [c,**], Yuan Chen [a,b,*]

[a] Chinese Herb Medicine Division, Zhejiang Agriculture and Forestry University, 666 Wusu Street, Lin'an 311300, PR China
[b] The State Key Laboratory of Subtropical Silviculture, Zhejiang Agriculture and Forestry University, 666 Wusu St, Lin'an 311300, PR China
[c] Zhejiang Key Laboratory for Laboratory Animal and Safety Research, Zhejiang Academy of Medical Sciences, PR China

ARTICLE INFO

ABSTRACT

Tripterygium wilfordii Hook *F.* (TWHF) is a Chinese traditional medicine with cardiac toxicities. However, the mechanism of acute cardiac toxicity is not very clear. By using patch clamp techniques, we found that 0.05 mg/ml and 0.1 mg/ml of the aqueous crude extract of TWHF inhibit $21.4 \pm 1.6\%$ and $86.7 \pm 5.7\%$ (n = 5) of hERG current Amplitudes (I_{hERG}) respectively. We further found that Celastrol, one of main components of TWHF, inhibits hERG with an IC_{50} of 0.83 μM. Additional mutagenesis studies show that mutations of T623A, S624A and F656A significantly alter the inhibition and S624A has the strongest effect, supported by our docking model. Our data suggest that inhibition of hERG channel activity by Celastrol contributed to TWHF cardiotoxicity.

1. Introduction

Tripterygium wilfordii Hook F. (TWHF) was first recorded in the earliest Chinese herb medicine book "Shennong Ben Cao Jing" (Li and Gao, 1991), also known as "Thunder of God vines". Despite its toxicity, TWHF has been developed into clinical drugs for immune regulation, anti-inflammation and anti-tumor (Cascao et al., 2017). Two licensed drugs, TWHF tablets and TWHF multi-glycosides tablets, have been authorized by China Food and Drug Administration for the treatment of inflammatory and autoimmune diseases, especially rheumatoid arthritis for over thirty years (Li et al., 2011; Lin et al., 1985).

TWHF contains hundreds of chemical constituents with Triptolide monomer most toxic (Xue et al., 2010). Triptolide can exert different toxic effects on heart, liver, bone marrow, lung, kidney (Liu et al., 2005). It impacts the reproductive systems and significantly reduces both testis and epididymis weights in male (Ni et al., 2008) and the relative weights of ovary and uterus in female (Huang et al., 2013; Liang et al., 2001; Liu

et al., 2011). Triptolide has also been found to induce hepatotoxicity (Liang et al., 2001; Shen et al., 2014; Wang et al., 2013), acute nephrotoxicity (Sun et al., 2013; Yang et al., 2012). Additionally, it has shown cardiotoxicities (Zhou et al., 2014).

Celastrol is another strong toxic component extracted from TWHF and demonstrates effects on the development of zebra fish embryo (Wang et al., 2011). It also causes heart dis-function to zebra fish embryo and significantly reduces heart rate with increase of concentration and duration of treatment (Wang et al., 2009). Early *in vitro* assay showed that in addition to potent inhibitory activity on both Kir2.1 and hERG potassium channels, Celastrol can alter the rate of ion channel transport and reduce channel density on the cell surface (Singer, 2006).

The first cardiac toxicity case of TWHF was reported in 1995. A previously healthy young man developed profound hypotension and abnormal ECG after ingestion of TWHF and died three days later (Chou et al., 1995). Since then, many case reports of cardiotoxicities of TWHF have been published (Chen, 1999; Wu, 1994). To explore the potential

---

* Corresponding author.
** Corresponding author.
E-mail addresses: zjsdgb@163.com (L. Wu), ychen@zafu.edu.cn (Y. Chen).
[1] Equal contributors.

mechanisms, both TWHF extract and TWHF glycosides have been studied and found to induce myocardial injury corresponding to histo-pathology change and cardiovascular function abnormality (Bai et al., 2011; Hua et al., 2011).

Cardiac arrhythmia is one kind of drug induced major cardiotoxicities. It is due to the irregularities of cardiac action potential (AP). AP of cardiac myocytes requires delicate balance activities among ion channels. Human ether-a-go-go related gene (hERG) potassium channel is one of these important channels. It responses to the repolarization and termination of AP. Either blockade of hERG channel or loss-of-function mutation of its genes can induce long QT syndrome (LQTS), showing a prolonged QT interval in the electrocardiogram which may cause fatal arrhythmias such as torsade de pointes (TdP) (Sanguinetti and Mitcheson, 2006). hERG channels are promiscuity and able to bind many different structures of chemicals (Wang and Mackinnon, 2017). In fact, most drug induced toxicity is due to inhibition of hERG channels historically. Therefore, hERG binding assays have become a standard safety screening requirement during the early stages of drug developments (Sanguinetti and Mitcheson, 2006). The case report aforementioned is an acute event and difficult attributed to abnormal cardiac development. The detailed mechanisms behind the event is still a mystery and whether TWHF extract or TWHF multi-glycosides tablets target hERG channels also lacks of report. Since inhibition to hERG channels is highly related to TdP and sudden death, we started to study TWHF effects on hERG channels.

Celastrol and Triptolide are two main active components in TWHF with strong pharmacological effects, and their pharmacological effects are similar to TWHF too. Thus, they were chosen for further mechanism studies against hERG channels. The results may guide us to safely use TWHF and develop new derivatives with high efficiency while low toxicity.

2. Methods

2.1. Cells

Human Embryonic Kidney (HEK) 293 cells with hERG stably expressed were routinely cultured in the solution with 10% (v/v) fetal bovine serum (FBS), 1% (v/v) P/S (100U Penicillin and 0.1 mg/ml streptomycin) and 100 μg/ml G418 (Xu et al., 2016). On the day before experiment, the cells were redistributed on glass cover slips lack of P/S and G418. Plasmid pCDNA3.1 contained the cDNA encoding the full-length of hERG gene. The hERG channels mutants, T623A, S624A, V625A, Y652A and F656A, were generated using KOD-Plus-Mutagenesis Kit (TOYOBO, OSAKA, Japan). And the mutant cDNAs were transient transfected into HEK293 cells by using Lipofectamine™ 2000. The cDNA encoding the CD8 receptor in pCDM8-NEO was used as a marker of the transfected cells (Chen et al., 2006). After 12 h, transfected cells were re-plated at low density (about 10% confluence) for electrophysiological recordings. The successfully transfected cells were identified by labeling with CD8-specific antibody-coated microspheres (Dynal, Oslo, Norway).

2.2. Preparation of Triptergium wilfordii Hook F. (TWHF) aqueous crude extract

100 g of dry root of Tripterygium was soaked in 800 ml distilled water for 30 min. TWHF was then heated and boiled for 40 min. The filtration was collected after TWHF was filtered. And the remaining raw TWHF material was boiled again for another 30min after adding 1000 ml water. The filtration was collected and combined with the previous one, heated and concentrated to an exact volume of 100ml. After cooling down to room temperature, the sample was reserved at 4 °C for further experiments.

2.3. Electrophysiology

The hERG channel currents were recorded by a whole cell patch clamp, which was filled with potassium aspartate solution (140 mM potassium aspartate, 10 mM HEPES, 5 mM Mg ATP, 2 mM $MgCl_2$, 11 mM EGTA; pH 7.3, adjusted with KOH base). The bath solution contained (mM) NaCl, 136; KCl, 4; $CaCl_2$, 1.8; $MgCl_2$, 1; Glucose, 10 and HEPES, 10; pH 7.3 with NaOH. All the chemicals were bought from Sigma. The extracellular solution flow was regulated by gravity. Celastrol and Triptolide (Sigma-Aldrich Corporation) was dissolved in DMSO and diluted 300-fold to their final concentrations except where noted. The recording electrodes had resistances of 2–3MΩ. The current curves were attained by PC 505B (Warner Instrument Corporation) clamp amplifier. The data were filtered at 2 kHz with protocol generated by Clampex. All experiments were performed at room temperature (25 °C).

2.4. Statistics analysis

Electrophysiological data were analyzed by Clampfit software (Version 10.4, Axon Instruments) and Origin 8.0 (OriginLab Corporation, US). IC_{50} value was obtained by fitting the concentration dependent data to the following equation, $I(\%) = 1/\{1+(IC_{50}/[D])^n\}$. In the equation, I% is percentage inhibition of current amplitudes; IC_{50} is the concentration of half maximal inhibition; [D] is the concentration of a compound and n is the hill coefficient. Figures were prepared with Origin Pro 8.0. All data are expressed as mean ± S.E.M., and statistical significance (P < 0.05) was determined using paired t-tests or t-tests. I–V relations were fit with single Boltzmann functions according to:

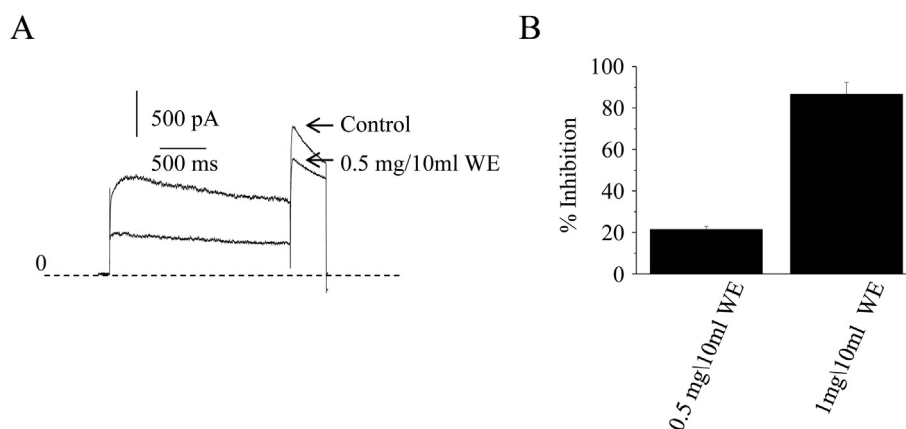$$I/I_{max} = (1+e^{-ZF\ (V-V1/2)/RT})^{-1}$$

Fig. 1. (A) Examples of current traces show the inhibition effects of the aqueous crude extract (ACE) (B) Bar graph shows the percentage inhibition of ACE at concentrations of 0.05 mg/ml and 0.1 mg/ml.
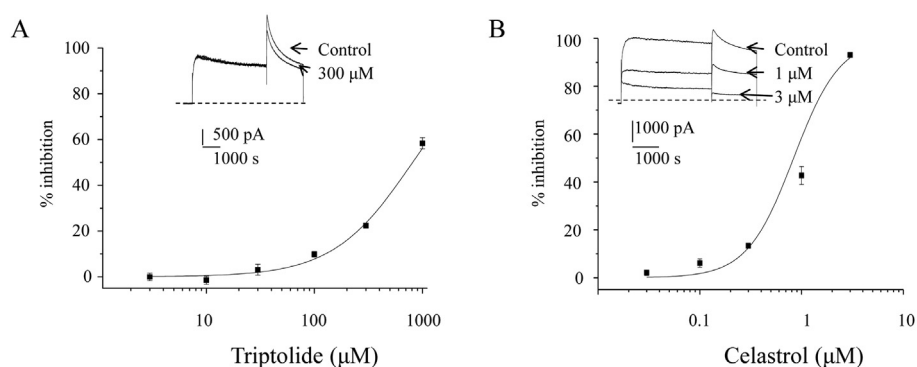
Fig. 2. Concentration dependent inhibition of Triptolide (A), and Celastrol (B). Insets are representative current traces. The IC_{50} value for Triptolide is 811.1 μM and for Celastrol 0.83 μM.
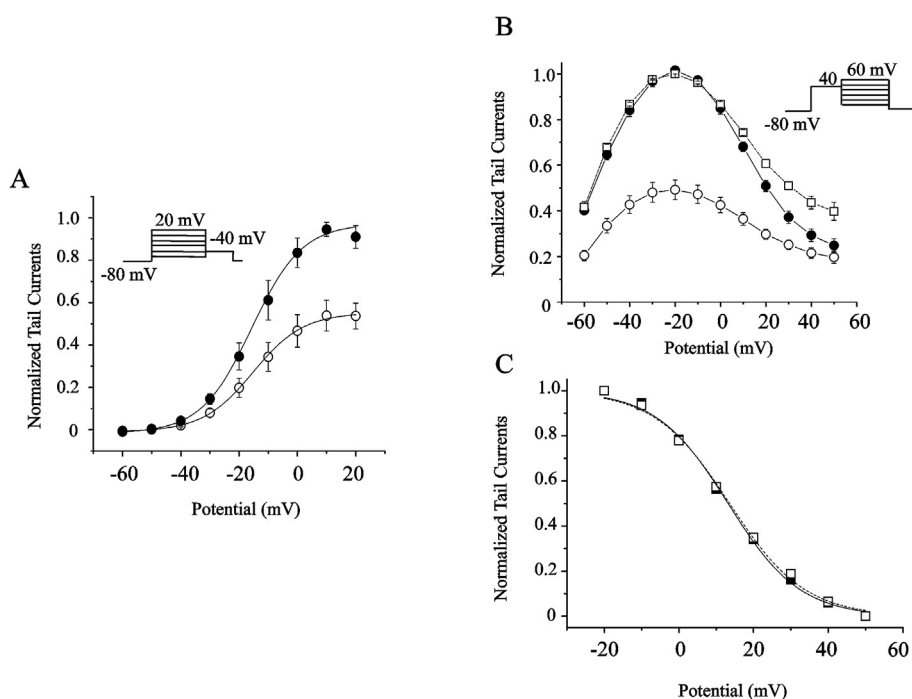

Fig. 3. (A) The steady state activation. The insert is the protocol. Prepulse duration is 4 s (●) represents the normalized control peak tail currents measured at different test voltages; (○) presents the normalized peak tail currents measured at different test voltages in presence of 1 μM Celastrol. (B) The steady state inactivation. The insert is the protocol. Prepulse duration is 4 s (●) represents the normalized control peak tail currents measured at different test voltages; (○) presents the normalized peak tail currents measured at different test voltages in presence of 1 μM Celastrol. □ presents the peak tail currents, normalized to the maximal peak tail currents in control, measured at different test voltages in presence of Celastrol. (C) The same as (B), the steady state inactivation is overlapping each other before and after 1 μM Celastrol. The data is normalized from its minimal to maximal peak tail currents before and after 1 μM Celastrol. Only right side of the peak tail currents is shown. (■) represents the normalized control peak tail currents measured at different test voltages; (□) presents the normalized peak tail currents measured at different test voltages in presence of 1 μM Celastrol.

where I/Imax is the normalized current, Z (slope) is the effective valence, $V_{1/2}$ is the half-activation voltage, F the Faraday's constant, R the gas constant, and T temperature in Kelvin.

2.5. Homology modeling

The cryo-EM structure of the human ether-a`-go-go-related potassium channel (hERG) homotetramer (PDB code: 5VA1) was downloaded from the Protein Data Bank (https://www.rcsb.org/) (Wang and MacKinnon, 2017). The final model was refined with 5000 steps of steepest descent minimization, followed by 5000 steps of conjugate gradient minimization using the CHARMm force field (MacKerell et al., 1998) and implicit solvent model (a generalized Born model with molecular volume) implemented in Discovery Studio (DS) molecular simulation package (version 2.5). Ramachandran plot was used to assess the quality of the refined model.

2.6. Induced fit docking

The 3D structures of celastrol were conducted using *Maestro* and optimized with *Macromodel* in Schrödinger with the OPLS force field (Kaminski et al., 2001). After that, celastrol was prepared with the *Ligprep*

module in Schrödinger. The protonated states and the tautomerization states of celastrol were produced. The refined model of hERG was chosen as the receptor in the docking calculations. The protonation states and partial charges of hERG were assigned with the *Protein Preparation Wizard* module in Schrödinger using the OPLS force field. The *Induced fit docking* (IFD) protocol was employed to predict the binding models of hERG in complex with the hERG channel. The flexibility of the channel in the binding site was determined using the rigid receptor docking (*Glide*). The active site was centered at the central cavity of the pore region of hERG (especially Thr623, Ser624, Val625, Tyr652 and Phe656) in each of the four subunits according to previous studies (Vandenberg et al., 2017). In the IFD calculations, the residues within 5 Å of celastrol was subjected to a conformational search and energy minimization, while the others were fixed. Finally, the best hERG-celastrol complexes with the top-ranked structures evaluated by the Glide XP scoring mode were chosen.

3. Results

3.1. Aqueous crude extractAqueous crude extracts of TWHF inhibit hERG channels

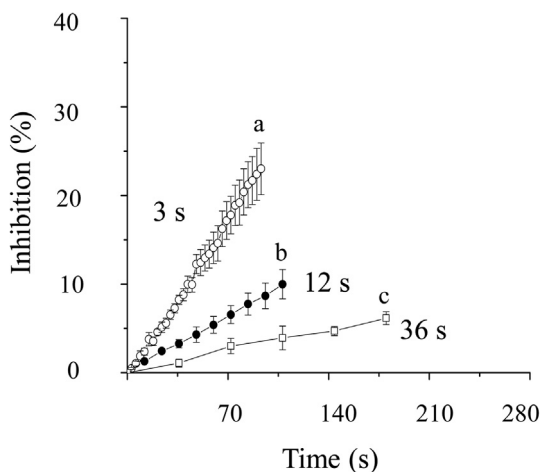Small amount of aqueous crude extracts (ACEs) was diluted into the

Fig. 4. Frequency dependence of Celastrol inhibition. (○) represents the percentage inhibition of 0.3μM Celastrol at a pulse interval of 3 s. (●) represents the percentage inhibition of 0.3μM Celastrol at a pulse interval of 12 s. (□) represents the percentage inhibition of 0.3μM Celastrol at a pulse interval of 36 s. Letters *a,b* and *c* are where the percentage inhibition is measured.
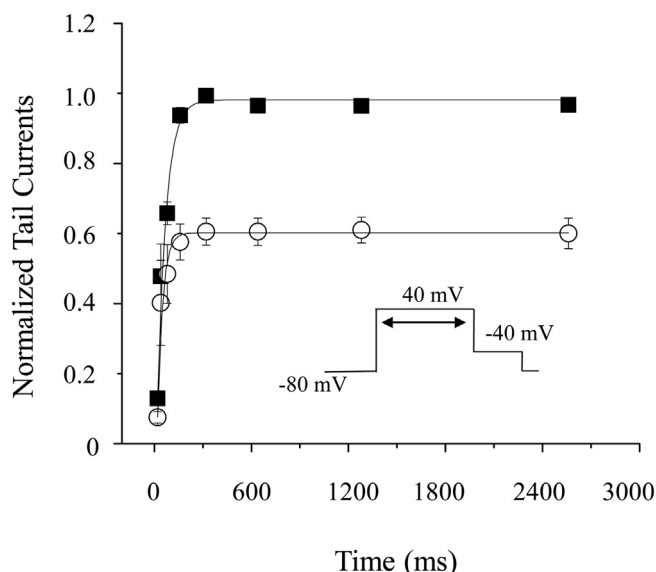

Fig. 5. Celastrol does not change the onset of inactivation. (■) represents the normalized control peak tail currents measured at different prepulse lengths; (□) represents the normalized peak tail currents measured at different prepulse lengths in presence of 1 μM Celastrol. Insert is the protocol.

extracellular solution to final concentrations of 0.5 mg and 1 mg per 10 ml. Using a standard protocol, we activated hERG currents by evoking cells with a 2-second test pulse to 40 mV from holding potential at -80 mV and then deactivating to -40 mV to obtain the tail currents. The results clearly showed hERG channels were inhibited by TWHF extracts. The lower ACEs concentration inhibited the hERG peak tail currents by 21.4 ± 1.6% (n = 5) while the higher concentration inhibits 86.7 ± 5.7% (n = 5) tail currents (Fig. 1).

3.2. Celastrol is a much stronger hERG channels inhibitor than Triptolide

Celastrol and Triptolide are two main active components of TWHF. Their activities presumably correlate to their pharmacological functions. Here, Celastrol was perfused directly to cells to examine its effects on I_{hERG}. Fig. 2B showed the inhibition effect by respective Celastrol concentration. At 0.03, 0.1, 0.3, 1, and 3 μM, we obtained 2.0 ± 1.1%, 6.1 ±

1.7%, 13.0 ± 1.0%, 42.7 ± 3.7% and 93.1 ± 1.0% inhibition respectively (n = 4). Fitting the curve yielded an IC_{50} of 0.83 μM. Triptolide was also examined against hERG channels (Fig. 2A). At 3, 10, 30, 100, 300 and 1000 μM, the average percentage inhibitions were 0 ± 1.7%, -1.5 ± 1.8%, 3.1 ± 2.4%, 9.9 ± 1.2%, 22.4 ± 1.0% and 58.3 ± 2.5% respectively (n = 4–6). This yielded an IC_{50} of 811 μM, a value of more than 800 fold higher than Celastrol. Based on these observations, we concluded that TWHF inhibits hERG channels mainly through Celastrol instead of Triptolide.

3.3. Celastrol does not alter the steady state activation and inactivation of hERG channels

To examine the effects of Celastrol on the steady state activation and inactivation of hERG channels, the normalized I–V relationship for I_{hERG} was measured at the end of depolarizing pulse of 10 mV. As shown in Fig. 3A, there was no obvious shift in the voltage dependence of activation. Before and after perfusion of 1μM Celastrol, the $V_{1/2}$ was -15.7 ± 1.07mV (n = 5) and -15.2 ± 0.46 mV (n = 5), and the slope was 8.66 ± 0.55 and 8.67 ± 0.22 respectively.

To examine the effect of Celastrol on voltage dependent activation of hERG channels, we normalized I–V relationships for peak tail currents. Both protocol and result were shown in Fig. 3. Clearly, at1μM Celastrol, the inhibition rates remained almost unchanged between 45.2-41.0% at voltage pulses between -30 mV to 20 mV. The result suggests that Celastrol inhibition on the channels is independent on the voltage.

To examine the effect on the steady state inactivation, the peaks of hERG currents were compared. At 1μM Celastrol, no shift was observed in the inactivation peaks since the normalized peaks overlapped each other. To better understand the steady state inactivation, we normalized the currents from the bottoms to the peaks for the treatments with or without 1μM Celastrol. As shown in Fig. 3C, after fitting the data by Boltzmann equation, we obtained similar $V_{1/2}$ values, 13.6 ± 0.6 vs 13.1 ± 0.5 mV, and unchanged slope of 0.04 ± 0.00 (n = 5). The data thus suggested that Celastrol does not change the steady state inactivation.

3.4. The inhibition of hERG channels by celastrol was frequency dependent

To investigate whether the blockade of hERG channels by Celastrol is frequency dependent, we used a test pulse of 0.5 s depolarizing steps to +40 mV from holding potential -80 mV in intervals of 3 s, 12s or 36 s in the presence of 0.3μM Celastrol. Although the inhibition would become stable eventually, the data indeed showed that the inhibition by Celastrol depends on the activation frequency. The maximal percentage inhibitions which were recorded at the last pulses for the interval of 3 s, 12s or 36 s were 23.0 ± 2.9%, 10.0 ± 1.7% and 6.2 ± 0.7% respectively (n = 4, p < 0.01). Fig. 4 shows that the percentage inhibition at 3-s interval is greater than that at 12 s interval, which is greater than that at 36 s interval. The data suggests that inhibition of Celastrol is frequency dependent.

3.5. Celastrol does not change the onset of hERG channel inactivation

With the protocol described in Fig. 5, hERG channels were monitored and activated with 20 ms, 40 ms, 80 ms, 160 ms, 320 ms and 640 ms depolarization steps to 40 mV at a pulse interval of 3 s. At 160 ms, the peak tail currents turned into steady. Further longer activation pulse (>160 ms) did not change the inhibition rate by 1μM Celastrol. This suggests that hERG channels are maximally activated at 160 ms. Furthermore, 1μM Celastrol treatment did not significantly change the time constants (50.6 ± 9.5 vs. 48.4 ± 18.9, n = 4; p > 0.05), suggesting that Celastrol blockade may not be sensitive to hERG channel inactivation (Suessbrich et al., 1997).
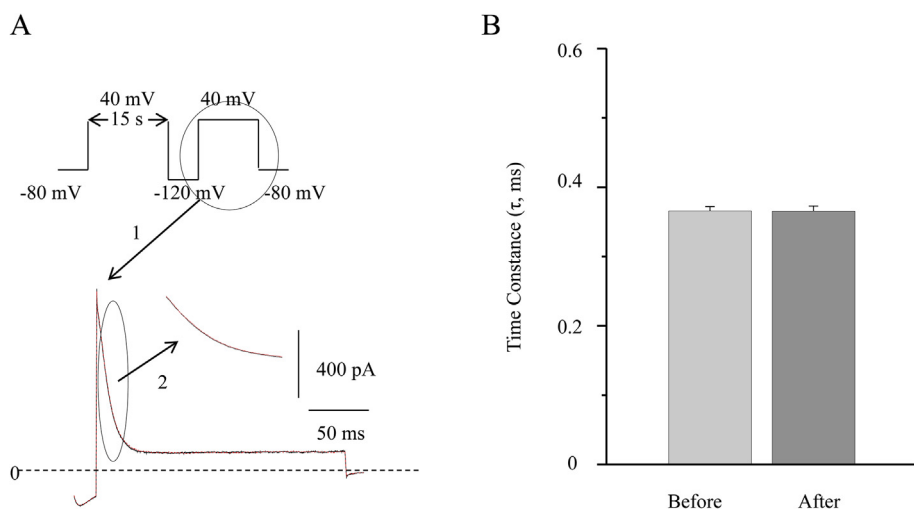
A

B

Fig. 6. Celastrol does not change the kinetics of hERG inactivation. (A) Up-panel is a voltage clamp pulse protocol. The holding potential is at -80 mV, the length of prepulse is 15 s at 40 mV, the test pulse is at 40 mV and between the prepulse and the test pulse is the briefly hyperpolarized pulse, which is at -120 mV for 20 ms. Bottom panel is the example current traces activated by the test pulses before and after 1 μM Celastrol. 1 and 2 indicate where the traces are from. (B) The bars indicate the decay time constants of inactivation kinetics. There is no significant changes in the presence or absence of 1μM Celastrol (n = 5, p > 0.05).
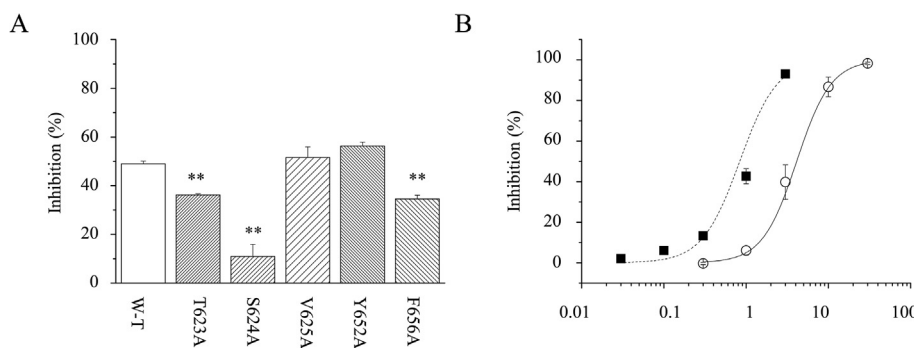
A

B

Fig. 7. Potential important Celastrol binding sites. (A) The bar graph suggests that T623, S624, and F656 are potential important binding sites, which are significantly sensitive to 1μM Celastrol. Among them, S624 locating near the pore helix is the most sensitive site. ** indicates p < 0.01 (B) Concentration dependent inhibition of Celastrol on mutant S624A. The IC_{50} value is 4.0 ± 0.3 μM. (○) presents the normalized inhibition measured against S624A hERG channels at different concentration of Celastrol. (■) same as Fig. 2B, represents the normalized inhibition against WT hERG channels measured at different concentration of Celastrol.
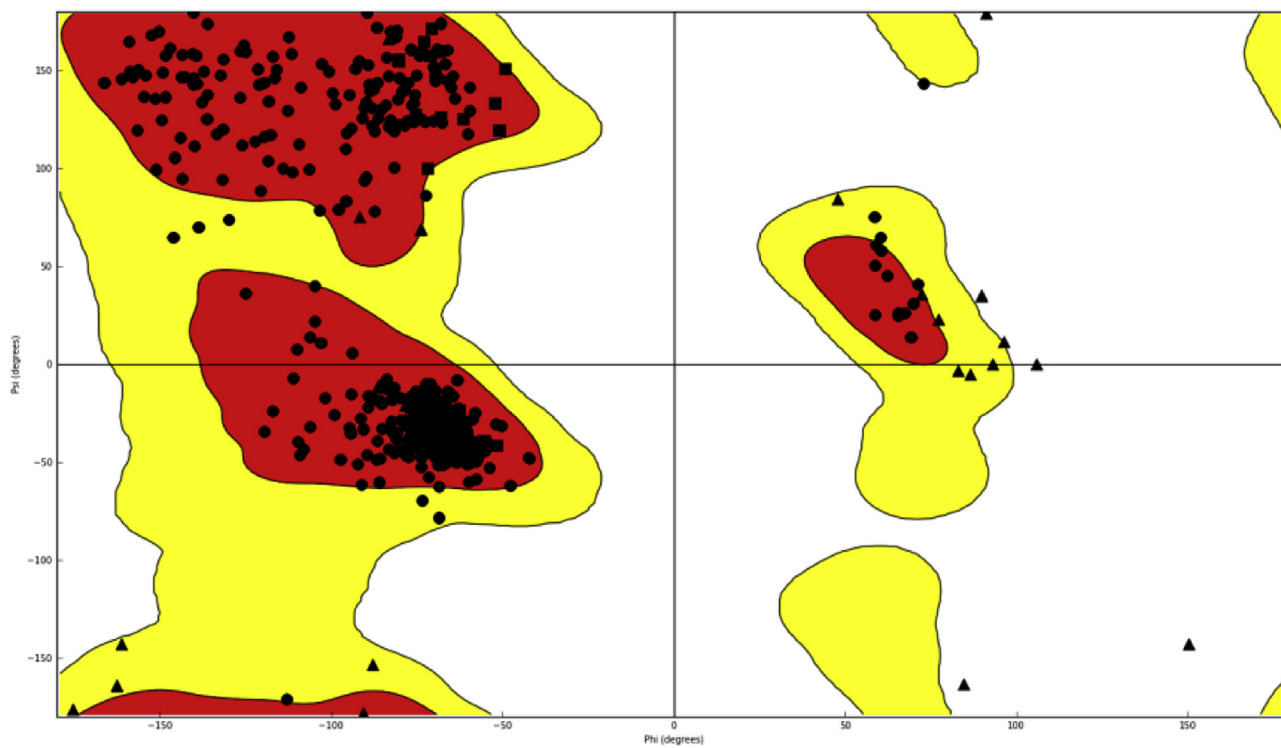

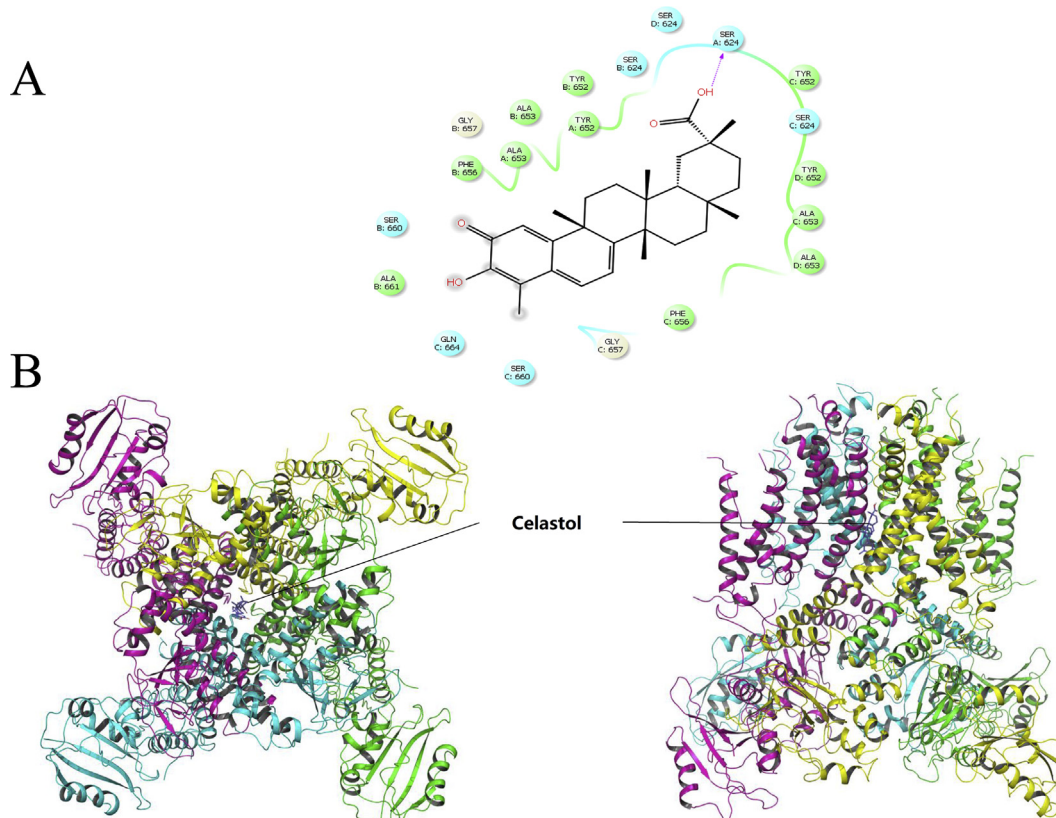**Fig. 8.** Ramachandran plot of the hERG channel homotetramer.

Fig. 9. (A) Induced-fit docking model of Celastrol in the active site of hERG. The residues in different domains are colored in light blue, green and grey respectively, and the Celastrol is colored in black. "→"shows the hydrogen bond between Celastrol and Ser624. (B) Top (left) and side (right) views of the docked ligands in complex with the hERG model. Domains I to IV are shown as cyan, purple, green and yellow ribbons, and Celastrol is represented as sticks and colored in royal blue.

3.6. Celastrol inhibition does not affect the inactivation kinetics of hERG channels

To investigate the effects of Celastrol on hERG inactivation kinetics, we adopted a voltage clamp pulse protocol as shown in Fig. 6. Following a test pulse of long depolarizing pulse (>15 s) at 40 mV from the holding potential at -80 mV, the membrane was briefly hyperpolarized to -120 mV for 20 ms, and then return to 40 mV hERG channels were then recovered from inactivation through 20 ms hyperpolarization, which did not cause a useful deactivation. Thus, the brief outward currents after the hyperpolarization can represent the hERG channels in a purely inactivated state. As shown in Fig. 6, the inactivation kinetics (the decay of the current amplitude) can be fit with an exponential function, yielding a time constant of 0.36 ± 0.006 ms and 0.37 ± 0.008 ms (n = 5) in the presence or absence of 1μM Celastrol respectively (p > 0.05). This unchanged time constant indicated that Celastrol does not affect the kinetics of hERG inactivation.

3.7. Residues T623, S624 and F656 in hERG channel involve celastrol binding

Studies have shown that hERG channel blockers are often found to bind within the inner cavity of the channel (Mitcheson et al., 2000a, b; Sanguinetti and Mitcheson, 2005; Witchel et al., 2004). According to previous studies, five amino acid sites were identified as potential drug binding sites and studied using Alanine-scanning mutagenesis. Among them, Y652 and F656 are inside the cavity with their side chains pointing towards the cavity center. The other three residues (T623, S624, and V625) locate near the pore helix (Fernandez et al., 2004). Previous study showed that their mutation to Alanine dramatically reduced the blockage or the sensitivities of drugs. To test whether Celastrol also interacts with the five residues, their Alanine mutants were individually and transiently

expressed. Currents of the mutant channels were compared with that of the wild type hERG channel in the presence of 1 μM Celastrol. The tail current amplitudes were measured at -40 mV. For mutants Y652A and F656A, the inhibitions were $56.3 \pm 1.6\%$ and $34.5 \pm 1.5\%$ (n = 5). For mutants T623A, S624A and V625A, the inhibitions were $36.2 \pm 0.4\%$ (n = 5), $10.9 \pm 5.0\%$ (n = 4) and $51.6 \pm 4.3\%$ (n = 4) respectively. As a comparison, inhibition to the wild type channel was $49.0 \pm 1.1\%$ (n = 4). Data analysis shows that, T623,S624 and F656 mutants have significantly reduced percentage inhibitions, comparing with WT (p < 0.01), among the five mutants (Fig. 7A), indicating the importance of three sites for Celastrol binding. S624A has strongest effect among the three mutants. To further confirm the effect of mutant S624A, a concentration response curve was examined against mutant S624A hERG channels (Fig. 7B). At 0.3, 1, 3, 10, and 30 μM of Celastrol, the average percentage inhibitions were $-0.3 \pm 5.7\%$, $6.1 \pm 2.2\%$, $39.8 \pm 8.4\%$, $86.7 \pm 4.8\%$, and $98.3 \pm 0.6\%$ respectively (n = 4–6). Its IC_{50} equals 4.0 ± 0.3μM, nearly 5 times higher than that of WT. The data suggests that S624 does have strong impacts on the channel inhibition by Celastrol.

3.8. Docking model reveals the S624 is the most effective binding site

To further examine the possible interaction at the atomic level between the celastrol and hERG channel, molecular docking of protein-ligands complexes was carried out. The transformation matrices of the 5VA1 PDB coordinate file was employed to generate the missing subunits of hERG, creating the fourfold symmetry required to build the hERG channel homotetramer, followed by the 10000 cycles minimization with the CHARMM force field and implicit solvent model in DS 2.5. The quality of the refined model was then evaluated by Ramachandran plot, which suggesting that the Phi/Psi angles of most residues (~90%) are within the reasonable ranges (Fig. 8). The IFD protocol was carried out to explore the molecular basis of the interaction between hERG and

celastrol. The best binding poses was chosen on the basis of the docking scores, and the surrounding residues of celastrol may have essential impact on the binding affinity between hERG and Celastrol.

According to the computational results, the docking score of binding affinity of Celastrol is -10.26. The superposition of the binding structures for Celastrol is shown in Fig. 8. Celastrol fits into the region formed by the IS6, IIS6, IIIS6 and IVS6 segments, and the plane of Celastrol is parallel to the pore axis. The carboxyl group of Celastrol can form hydrogen bonds with Ser624 in a subunit of hERG channel homotetramer (Fig. 9). Experiments above showed that mutant S624A most significantly reduced the inhibition of Celastrol, which is consistent with the docking results. Although the alleviating effects by T623A and F656A mutants were not directly supported by the docking results, the two mutants might shift local structure of hERG as the sidechains of T623 and F656 are larger than Alanine, and thus could reduce the inhibition.

4. Discussion

TWHF has been long reported to cause cardiac toxicity but it is not known how the toxicity is induced. The difficulty of the study might be due to the existence of hundreds of compounds in TWHF not mention there are also many ways to cause cardiac toxicity. Among the many factors, the amount of a compound and its strength to cause cardiac toxicity are often most important. Since Triptolide and Celastrol are two main ingredients of TWHF and both show functions and their toxicities are correlated with TWHF, they were chosen to be investigated in order to understand the possible mechanisms of cardiac toxicity of TWHF by focusing on the hERG channel inhibition. Our data indicates that the aqueous crude extract of TWHF does inhibit hERG channels and the inhibition is likely concentration dependent. Thus, the data suggests that cardiac toxicity of TWHF could go through hERG inhibition. Between the two main components tested, Triptolide is a weak hERG channel inhibitor with an IC_{50} of 811 μM, suggesting that Triptolide does not play a major role of inhibiting hERG channels by TWHF. However, Celastrol showed a strong inhibition to hERG channels with an IC_{50} of 0.83 μM. An IC_{50} less than 1 μM can be considered as very strong against different type of ion channels among the compounds we have screened from plants (Kan et al., 2017; Xu et al., 2016). We have not seen any IC_{50} less than 1μM from over 100 of these type compounds so far.

Celastrol inhibition shows a feature of highly frequency or use-dependent. Increase of the stimulation frequency or decrease of the pulse interval can significantly enhance the inhibition. There are two possibilities to explain the phenomenon, inactivation dependent mechanism or trapping mechanism. Since our data does not support frequency inhibition which is inactivation dependent, a plausible explanation of the phenomenon is the trapping mechanism, which means that Celastrol molecules can enter into the pore of the channels easily but difficulty to get off from the pore. Thus, Celastrol is a long-term resident in the pore region, thereby showing stronger inhibition at hERG channels. The fact that the inhibition of Celastrol changes neither the steady state of activation nor the steady state of inactivation also indirectly supports the idea that Celastrol directly blocks the channels.

Our mutagenesis data suggests that Celastrol directly blocks hERG channels by binding the pore region of the channels. Among the five mutant residues, three of them, T623A, S624A and F656A, significantly reduce the inhibition of Celastrol. Among the three, S624A has the strongest effect, suggesting S624 is the most important binding site. The mutant data is also supported by our docking model. hERG channel is constructed by four identical α subunits. It is a homotetramer. There are total four S624 residues. The model suggests that three of four S624 contact with Celastrol. Among the three, one of them makes hydrogen connection with Celastrol molecules. The model explains the reason very well that S624A makes the most reduction of Celastrol inhibition and indicts that Celastrol inhibits hERG channels by directly blocking the channels.

Celastrol has many pharmacological activities. However, the IC_{50} or

EC_{50} of its activities is close to its IC_{50} of hERG inhibition, reflecting the safety window is small. For example, 3μM Celastrol, which is three times less potent to its hERG inhibition IC_{50}, was able to induce apoptosis or inhibit osteosarcoma cells (Chen et al., 2017; Huang et al., 2015). Some of its pharmacological activities are stronger. For example, 0.5 and 1μM of Celastrol could inhibit the metastasis of cultured esophageal cancer cells (Xu and Wu, 2015). It was also reported that Celastrol reduced damages caused by oxidation at 0.1–1μM (Li et al., 2016). Considering 0.3μM Celastrol has about 13% inhibition of hERG from our data, these pharmacological activities are pretty much overlap with cardiac toxicity caused by hERG channel inhibitions. Autoimmune disease is the most important therapeutic target of Celastrol. However, Celastrol shows significant roles in preventing autoimmune diseases but still need 1–10 μM concentrations to function at cellular level (Yuan, 2017) and 400 μg/kg to 3 mg/kg to exhibit anti-immune effect in vivo (Li et al., 2008; Wan et al., 1991). These concentrations also match with the strength of its hERG inhibition (Chun-Xing et al., 2017).

In conclusion, Celastrol shows a strong inhibition of hERG channels by directly blocking the pore region. Considering Celastrol is one of TWHF main components and has in many aspects to TWHF, a potential mechanism of cardiac toxicity of TWHF is likely due to hERG channel blockade by Celastrol. Additionally, our data suggests that Celastrol has a very narrow therapeutic safety window. Since Celastrol is a main ingredient of TWHF and represents many effects of TWHF, TWHF might have a narrow safety window too. Considering varied genetic background among individuals (Ando et al., 2011), some of patients may be much more sensitive to Celastrol as an hERG blocker, patients who are using TWHF glycosides tablets should be strictly guided by professional doctors.

Declarations

Author contribution statement

Wei Zhao: Performed the experiments; Analyzed and interpreted the data.

Liping Xiao, Lanying Pan, Yanting Zhang, Dian Zhong, Xuanfu Ke, Jianwei Xu, Fumin Cao: Performed the experiments; Analyzed and interpreted the data; Contributed reagents, materials, analysis tools or data.

Liren Wu, Yuan Chen: Conceived and designed the experiments; Wrote the paper.

Competing interest statement

The authors declare no conflict of interest.

Additional information

No additional information is available for this paper.

References

Ando, F., Kuruma, A., Kawano, S., 2011. Synergic effects of beta-estradiol and erythromycin on hERG currents. J. Membr. Biol. 241, 31–38.

Bai, J., Jiang, Y., Sun, X., Li, H., Lv, H., Liu, S., et al., 2011. Effects of *Triptergium wilfordii* extract on acute injury of rat heart. Pharmacol. Clin. China Mater. Med. 27, 89–93.

Cascao, R., Fonseca, J.E., Moita, L.F., 2017. Celastrol: a spectrum of treatment opportunities in chronic diseases. Front. Med. 4, 69–87.

Chen, Y., Yunsheng, O.U., Tao, Y., Yin, H., Huang, Q., Zhong, S., et al., 2017. Celastrol promotes apoptosis of human osteosarcoma HOS cells through endoplasmic reticulum stress pathway. Tumor 37, 901–908.

Chen, Y.H., 1999. A report of 3 cases of cardiogenic shock induced by acute *Tripterygium wilfordii* poisoning. Fujian Med. J. 21, 56-56.

Chen, Y., Yu, F.H., Surmeier, D.J., Scheuer, T., Catterall, W.A., 2006. Neuromodulation of Na$^+$ channel slow inactivation via camp-dependent protein kinase and protein kinase c. Neuron 49, 409–420.

Chou, W.C., Wu, C.C., Yang, P.C., Lee, Y.T., 1995. Hypovolemic shock and mortality after ingestion of *Tripterygium wilfordii* Hook F.: a case report. Int. J. Cardiol. 49, 173–177.

Chun-Xing, L.I., Tai-Sheng, L.I., Zhu, Z., Xie, J., Wei, L., Pharmacy, D.O., 2017. Determination of tripterine concentration in plasma of healthy volunteers and HIV-infected patients by methods of UPLC-MS/MS. J. Tradit. Chin. Med. Pharmal. 32, 814–818.

Fernandez, D., Ghanta, A., Kauffman, G.W., Sanguinetti, M.C., 2004. Physicochemical features of the HERG channel drug binding site. J. Biol. Chem. 279, 10120–10127.

Hua, L.I., Tang, N.P., Jing, M.A., Chen, C.X., 2011. Study on the cardiotoxicity of *Tripterygium wilfordii* glycosides in Beagle dogs. World Clin. Drugs 4, 219–224.

Huang, Z., Shao, L., Yangping, R., 2015. Celastrol induces caspase-dependent apoptosis through ROS/JNK pathway in Saos-2 cells. Chin. J. Pathophysiol. 31, 1457–1461.

Huang, Z.J., Que, H.Q., Zhu, H., Qian, L.P., 2013. Research progress in toxicity of triptolide on reproductive system. Drug Eval. Res. 3, 224–227.

Kaminski, G.A., Friesner, R.A., Tirado-Rives, J., Jorgensen, W.L., 2001. Evaluation andeparametrization of the OPLS-AA force field for proteins via comparison with accurate quantum chemical calculations on peptides. J. Phys. Chem. B 105, 6474–6487.

Kan, L.D., Zhao, W., Pan, L.Y., Xu, J.W., Chen, Q.M., Xu, K., et al., 2017. Peimine inhibits hERG potassium channels through the channel inactivation states. Biomed. Pharmacother. 89, 838–844.

Li, F., Li, Y.J., Li, Q.X., GuoYH, 2016. The inhibitive effects of celastrol on LDL oxidation and HAEC cell oxidative damage. Chin. Pharmacol. Bull. 32, 1578–1584.

Li, J., Lu, Y., Xiao, C., Lu, C., Niu, X., He, X., et al., 2011. Comparison of toxic reaction of *Tripterygium wilfordii* multiglycoside in normal and adjuvant arthritic rats. J. Ethnopharmacol. 135, 270–277.

Li, W.M., Gao, Y., 1991. Progress in the chemistry and pharmacology of *Tripterygium wilfordii*. Chin Tradit. Pat.Med. 9, 34–35.

Liang, L., Wang, Z., Huang, G., 2001. The influence of Triptolide sub-chronic intoxication on kidney and testicle in mice. Acta Univ. Med. Tangji 30, 214–217.

Lin, L., Jiang, J.M., Dai, H.Z., 1985. Introduce a new anti-inflammatory drug in our country- TWH glycoside tablets. Jiangsu Med. J. 3, 39–40.

Liu, J., Jiang, Z., Liu, L., Zhang, Y., Zhang, S., Xiao, J., et al., 2011. Triptolide induces adverse effect on reproductive parameters of female Sprague-Dawley rats. Drug Chem. Toxicol. 34, 1–7.

Liu, M.X., Dong, J., Yang, Y.J., Yang, X.L., Xu, H.B., 2005. Progress in research on triptolide. China J. Chin. Mater. Med. 30, 170–174.

Li, M.Q., Dou, J., Wei, D.U., Li, X.Y., Lin, J., 2008. Effects of tripterine on the immunosuppression action and expression of IL-6 mRNA in mice. Chin. J. Clin. Pharmacol. Therapeut. 13 (2), 158–163.

MacKerell, A.D., Bashford, D., Bellott, M., Dunbrack, R.L., Evanseck, J.D., Field, M.J., et al., 1998. All-atom empirical potential for molecular modeling and dynamics studies of proteins. J. Phys. Chem. B 102, 3586–3616.

Mitcheson, J.S., Chen, J., Lin, M., Culberson, C., Sanguinetti, M.C., 2000a. A structural basis for drug-induced long QT syndrome. Proc. Natl. Acad. Sci. U. S. A. 97, 12329–12333.

Mitcheson, J.S., Chen, J., Sanguinetti, M.C., 2000b. Trapping of a methanesulfonanilide by closure of the HERG potassium channel activation gate. J. Gen. Physiol. 115, 229–240.

Ni, B., Jiang, Z., Huang, X., Xu, F., Zhang, R., Zhang, Z., et al., 2008. Male reproductive toxicity and toxicokinetics of triptolide in rats. Arzneimittelforschung 58, 673–680.

Sanguinetti, M.C., Mitcheson, J.S., 2005. Predicting drug-hERG channel interactions that cause acquired long QT syndrome. Trends Pharmacol. Sci. 26, 119.

Sanguinetti, M.C., Mitcheson, J.S., 2006. hERG potassium channels and cardiac arrhythmia. Nature 440 (7083), 463–469.

Shen, G., Zhuang, X., Xiao, W., Kong, L., Tan, Y., Li, H., 2014. Role of CYP3A in regulating hepatic clearance and hepatotoxicity of triptolide in rat liver microsomes and sandwich-cultured hepatocytes. Food Chem. Toxicol. 71, 90–96.

Singer, H., 2006. Chronic inhibition of cardiac Kir2.1 and HERG potassium channels by celastrol with dual effects on both ion conductivity and protein trafficking. J. Biol. Chem. 281, 5877–5884.

Suessbrich, H., Schonherr, R., Heinemann, S.H., Attali, B., Lang, F., Busch, A.E., 1997. The inhibitory effect of the antipsychotic drug haloperidol on HERG potassium channels expressed in Xenopus oocytes. Br. J. Pharmacol. 120, 968–974.

Sun, L., Li, H., Huang, X., Wang, T., Zhang, S., Yang, J., et al., 2013. Triptolide alters barrier function in renal proximal tubular cells in rats. Toxicol. Lett. 223, 96–102.

Vandenberg, J.I., Perozo, E., Allen, T.W., 2017. Towards a structural view of drug binding to hERG K(+) channels. Trends Pharmacol. Sci. 38, 899–907.

Wan, L., Yang, S., Wang, J., Zhu, M., Ge, J., Li, X., 1991. Inhibiting effect of celastrol on immune responses. Pharmacol. Clin. China Mater. Med. 7, 18–21.

Wang, J., Jiang, Z., Ji, J., Wang, X., Wang, T., Zhang, Y., et al., 2013. Gene expression profiling and pathway analysis of hepatotoxicity induced by triptolide in Wistar rats. Food Chem. Toxicol. 58, 495–505.

Wang, S., Liu, K., Wang, X., He, Q., Chen, X., 2011. Toxic effects of celastrol on embryonic development of zebrafish (*Danio rerio*). Drug Chem. Toxicol. 34, 61–65.

Wang, S.F., Liu, K.C., Wang, X.M., He, Q.X., Han, L.W., Hou, H.R., 2009. Preliminary study on cardiotoxicity of celastrol to zebrafish embryo. Chin. Pharmacol. Bull. 25, 634–636.

Wang, W., Mackinnon, R., 2017. Cryo-em structure of the open human, ether-à-go-go-related k+, channel herg. Cell 169 (3), 422–430.

Witchel, H.J., Dempsey, C.E., Sessions, R.B., Perry, M., Milnes, J.T., Hancox, J.C., et al., 2004. The low-potency, voltage-dependent HERG blocker propafenone–molecular determinants and drug trapping. Mol. Pharmacol. 66, 1201–1212.

Wu, M.Z., 1994. 1 case of arrhythmia caused by *Tripterygium wilfordii* poisoning. Heilongjiang J. Tradit. Chin. Med. 5, 44–45.

Xu, J., Wu, C.L., 2015. Anti-metastasis of celastrol on esophageal cancer cells and its mechanism. Acta Physiol. Sin. 67, 341–347.

Xu, J., Zhao, W., Pan, L., Zhang, A., Chen, Q., Xu, K., et al., 2016. Peimine, a main active ingredient of fritillaria, exhibits anti-inflammatory and pain suppression properties at the cellular level. Fitoterapia 111, 1–6.

Xue, J., Jia, X.B., Tan, X.B., Chen, Y., Zhang, L.Y., 2010. Chemical constituents of *Triptergium wilfordi* Hook.f and its toxicity. Chin. J. Tradit. Chin. Med. Pharmal. 25, 726–733.

Yang, F., Ren, L., Zhuo, L., Ananda, S., Liu, L., 2012. Involvement of oxidative stress in the mechanism of triptolide-induced acute nephrotoxicity in rats. Exp. Toxicol. Pathol. 64, 905–911.

Yuan, K., 2017. Study on the Mechanism of Triptolide and Celastrol Ameliorating Rheumatoid Arthruis by Inhibiting Neutrophil Mediated inflammation. Doctoral Dissertation. Beijing University of Chinese Medicine.

Zhou, J., Xi, C., Wang, W., Fu, X., Liang, J., Qiu, Y., et al., 2014. Triptolide-induced oxidative stress involved with Nrf2 contribute to cardiomyocyte apoptosis through mitochondrial dependent pathways. Toxicol. Lett. 230, 454–466.